Applied Physics Letters

RESEARCH ARTICLE | NOVEMBER 15 2022

Mg-implanted vertical GaN junction barrier Schottky rectifiers with low on resistance, low turn-on voltage, and nearly ideal nondestructive breakdown voltage

Maciej Matys ✉; Kazuki Kitagawa; Tetsuo Narita; ... et. al

Appl. Phys. Lett. 121, 203507 (2022)
https://doi.org/10.1063/5.0106321

AIP Publishing

Applied Physics Letters ARTICLE scitation.org/journal/apl

Mg-implanted vertical GaN junction barrier Schottky rectifiers with low on resistance, low turn-on voltage, and nearly ideal nondestructive breakdown voltage

Cite as: Appl. Phys. Lett. **121**, 203507 (2022); doi: 10.1063/5.0106321
Submitted: 28 June 2022 · Accepted: 1 November 2022 ·
Published Online: 15 November 2022

Maciej Matys,[1,a)] Kazuki Kitagawa,[2] Tetsuo Narita,[3] Tsutomu Uesugi,[1] Jun Suda,[1,2] and Tetsu Kachi[1,a)]

AFFILIATIONS

[1]IMaSS Nagoya University, Nagoya 464-8601, Japan
[2]Department of Electronics, Graduate School of Engineering, Nagoya University, Nagoya 464-8603, Japan
[3]Toyota Central R&D Labs., Inc., Nagakute, Aichi 480-1192, Japan

[a)]**Authors to whom correspondence should be addressed:** matys@imass.nagoya-u.ac.jp and kachi@imass.nagoya-u.ac.jp

ABSTRACT

Vertical GaN junction barrier Schottky (JBS) diodes with superior electrical characteristics and nondestructive breakdown were realized using selective-area p-type doping via Mg ion implantation and subsequent ultra-high-pressure annealing. Mg-ion implantation was performed into a 10 μm thick Si-doped GaN drift layer grown on a free-standing n-type GaN substrate. We fabricated the JBS diodes with different n-type GaN channel widths $L_n = 1$ and 1.5 μm. The JBS diodes, depending on L_n, exhibited on-resistance (R_{ON}) between 0.57 and 0.67 mΩ cm^2, which is a record low value for vertical GaN Schottky barrier diodes (SBDs) and high breakdown (BV) between 660 and 675 V (84.4% of the ideal parallel plane BV). The obtained low R_{ON} of JBS diodes can be well explained in terms of the R_{ON} model, which includes n-type GaN channel resistance, spreading current effect, and substrate resistance. The reverse leakage current in JBS diodes was relatively low 10^3–10^4 times lower than in GaN SBDs. In addition, the JBS diode with lower L_n exhibited the leakage current significantly smaller (up to reverse bias 300 V) than in the JBS diode with large L_n, which was explained in terms of the reduced electric field near the Schottky interface. Furthermore, the JBS diodes showed a very high current density of 5.5 kA/cm^2, a low turn-on voltage of 0.74 V, and no destruction against the rapid increase in the reverse current approximately by two orders of magnitude. This work demonstrated that GaN JBS diodes can be strong candidates for low loss power switching applications.

Vertical gallium nitride (GaN) power diodes are strong candidates for low loss power switching applications due to their low on-resistance (R_{ON}) and high breakdown voltage (BV).[1–12] In particular, owing to recent progress in fabrication of a freestanding GaN substrate, it was possible to realize high-quality vertical GaN p–n diodes.[13–19] Despite these excellent results, GaN p–n diodes exhibited a relatively large turn-on voltage ($V_{ON} \sim 3$) originating from the bandgap of GaN, which limited their practical applications due to power loss. On the other hand, Schottky barrier diodes (SBDs) can provide low V_{ON} (typically < 1V) due to the Schottky barrier interface. Nevertheless, SBDs suffer from the high off-state reverse leakage current due to thermionic-field emission (TFE) at the Schottky interface. The leakage currents of SBDs can be greatly reduced by the application of the junction barrier Schottky (JBS) structure. Additionally, the JBS structure can also provide an excellent avalanche capability due to the p–n junction, which is important for operating in a switching environment.

However, realization of the JBS structure for GaN is a challenging issue because of inefficiency of selective-area p-type doping technology. The first vertical Mg-implanted GaN JBS diodes obtained by a multicycle rapid thermal annealing (RTA) method exhibited high BV over 600 V but a very large R_{ON} (>100 mΩ cm^2).[20] Devices fabricated using this approach were improved by Zhang *et al.*[21] who reported vertical Mg-implanted GaN JBS diodes with the BV of 500–600 V and the R_{ON} of 1.7 mΩ cm^2. However, the destructive breakdown occurred at the Schottky contact edge, probably due to the low Mg activation ratio. Recently, Fu *et al.*[22] reported the avalanche capability in the Mg-implanted GaN JBS diodes obtained by the multicycle RTA method,

but R_{ON} was still high ($\sim$3 mΩ cm^2) as for the BV of 600–800 V. Due to the lack of effective Mg implantation technology, the other processes or structures were employed to GaN SBDs such as the vertical regrown JBS (RJBS),[23] trench JBS structure (TJBS),[24,25] or trench MOS barrier Schottky (TMBS) structure.[26,27] They exhibit very interesting properties, like keeping low leakage currents at high temperatures (TMBS structures), but they need the specific design and/or complex technological processes. On the other hand, Mg-ion implantation technology can offer flexible/simplified device design and reduced device fabrication complexity.

Compared to silicon carbide (SiC) JBS rectifiers, the GaN JBS diodes represent an early stage of development. Thus, the ability to realize high performance vertical GaN JBS diodes can bring GaN power electronics to the next level. Recently, our group fabricated various Mg-implanted GaN based edge termination structures[28,29] using an ultra high-pressure annealing (UHPA) method,[30–33] which ensured a high Mg activation ratio. In this Letter, we fabricated the Mg-implanted GaN vertical JBS diodes using the UHPA process and demonstrated their superior electrical characteristics and nondestructive breakdown.

Figure 1(a) shows the schematic cross-sectional image of the Mg-implanted vertical GaN JBS diodes. These devices were fabricated using a 10 μm thick silicon (Si)-doped GaN drift layer grown on free-standing GaN (0001) substrates prepared via hydride vapor phase epitaxy. The threading dislocation density was relatively low of the order of 10^6 cm^{-2}. The effective donor concentration (N_d) of the drift layer was estimated to be $\approx 2.5 \times 10^{16}$ cm^{-3} from the capacitance–voltage measurements. The JBS diodes with different n-GaN channel widths (L_n) were designed [see Fig. 1(a)]: $L_n = 1.5$ μm (JBS A) and $L_n = 1.0$ μm (JBS B). The width of the implanted p-type region (L_p) for both JBS diodes was designed to be 2 μm. The thickness of the drift layer was chosen as 10 μm in order to avoid the punch-through phenomenon (according to Ref. 34, for $N_d = 2.5 \times 10^{16}$ cm^{-3}, the non-punch-through drift layer should have the thickness larger than 5 μm).

The first step of the fabrication process was etching of an 1 μm thick SiO_2 mask in order to prepare the chosen regions for the implantation. Subsequently, the Mg ions were implanted with the energy of 20 and 180 keV at the respective dosages of 5×10^{14} and 8×10^{13} cm^{-2} at a tilt angle of 7°. Such a combination of the Mg energy and dosages leads to creation of a high p^+ region near the surface with the Mg concentration ([Mg]) of 10^{20} cm^{-3} and 0.22 μm thick box profile[35] with the average [Mg] of 4.5×10^{18} cm^{-3} according to the Monte Carlo (MC) simulations[36] [see Fig. 1(b)]. After implantation and mask removal, the UHPA process was conducted under an N_2 pressure of 500 MPa at a temperature of 1300 °C for 30 min at Japan Ultra-High Temperature Materials Research Institute in Ube City, Yamaguchi Prefecture, Japan. The Mg depth profile estimated by SIMS after the UHPA process has been shown in Fig. 1(b). The experimental Mg-depth profile extended more deeply in GaN than those predicted by MC simulations due to Mg diffusion,[37,38] which occurred during the UHPA process. The estimated width of the experimental Mg box profile was 0.44 μm with the average [Mg] of 1.18×10^{18} cm^{-3} [Fig. 1(b)]. After the UHPA process, the Ti/Al/Ni/Au Ohmic contacts were deposited on the substrate at 475 °C, and in the last step, the Ni/Au Schottky contacts were formed on the top. The JBS diodes were formed in a square shape with rounded corners as can be seen in the optical image shown in Fig. 1(c). The device active area contained

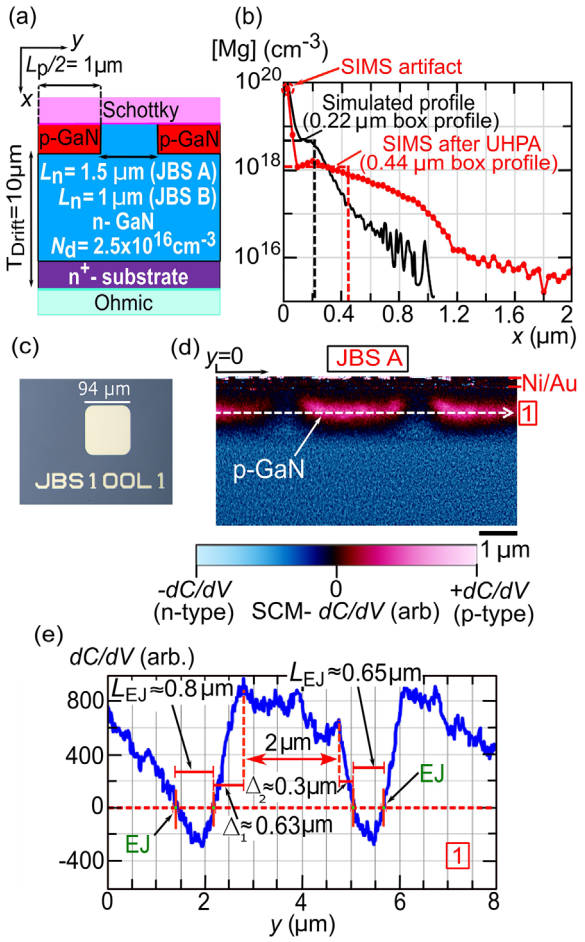

FIG. 1. (a) Schematic cross section of the JBS diodes, (b) SIMS depth profile of [Mg] together with the simulated [Mg] depth-profile, (c) optical image of the fabricated JBS diode, (d) SCM image of JBS A, and (e) linear profile of *dC/dV* obtained along line 1 from the SCM image. The high [Mg] peak on the surface [Fig. 1(b)] is probably due to a SIMS artifact.

periodically placed n-type and p-type regions, whose numbers of replications were 17 and 20 for JBS A and B, respectively.

The strong contrast between p-type and n-type regions was observed at the cross-sectional scanning capacitance microscopy (SCM) image [see Fig. 1(d)], which indicates a conversion of the n-type GaN region into p-type one. Figure 1(e) shows the linear profile of $\frac{dC}{dV}$ along line 1 from the SCM image of JBS A [Fig. 1(d)]. The electrical junction (EJ) locations,[39] i.e., points where the free electron and hole concentrations are equal (or points where the Fermi level is located at the midgap) can be clearly recognized. For JBS A, according to the TCAD simulations (see the supplementary material), the distance between EJ points (L_{EJ}) should be 1.2 μm, which is larger than experimental $L_{EJ} = 0.65$–0.8 μm [Fig. 1(e)]. This discrepancy can be due to the UHPA Mg lateral diffusion, which leads to shrinking of L_n (and expanding L_p) and/or not accurate EJ location estimation in the SCM measurements. In particular, it was shown that the EJ location in SCM measurements can be moved due to the AC tip bias.[39–41]

To estimate the EJ error location, we compared two regions Δ_1 and Δ_2 [see Fig. 1(e)], which roughly reflect expanding of L_p from the original size 2 μm. If the Mg lateral diffusion would be only responsible for reducing L_{EJ}, $\Delta_1 = \Delta_2$. (Mg diffusion is expected to be similar in both directions.) In our case, $\Delta_1 \gg \Delta_2$, which is likely due to the influence of the AC tip bias on the EJ location. Thus, the error of the EJ location can be estimated as: $\frac{\Delta_1-\Delta_2}{2} \approx 0.165$ μm. This means that the true L_{EJ} is $L_{EJ} = 0.98$ μm $(0.65 + 2 \times 0.165)$ and $L_{EJ} = 1.13$ μm $(0.8 + 2 \times 0.165)$. (We assumed that the true L_{EJ} should be larger then that obtained from the measurement because the AC tip bias enhances the depletion region.[40]) However, the determined L_{EJ} is still smaller than theoretical $L_{EJ} = 1.2$ μm, which indicates the presence of Mg lateral diffusion with a range L_R between 0.11 and 0.035 μm. Due to the Mg lateral diffusion, L_n is reduced by $2 \times L_R$ (L_p expands by $2 \times L_R$), and it is equal to 1.28–1.43 and 0.78–0.93 μm for JBS A and B, respectively.

The room temperature forward (I_F–V_F) and reverse (I_R–V_R) current–voltage characteristics were carried out using an Agilent B1505A semiconductor analyzer. The representative linear-scale I_F–V_F and the differential R_{ON}–V_F characteristics of JBS A and B as well as the Schottky barrier diode (SBD) are shown in Fig. 2(a). Note that I_F in Fig. 2(a) is normalized with respect to the total device active area (Schottky electrode area) equal to 8.6×10^{-5} cm^2. Unfortunately, the implanted pn diodes exhibited very low I_F due to the poor Ohmic contacts to implanted p-GaN, and thus, they were not shown in Fig. 2(a). The reason for poor Ohmic contacts to implanted p-GaN is likely low Mg concentration near the surface after the UHPA process [see Fig. 1(b)]. At $V_F = 1.5$–1.6 V, the JBS A and B exhibited the minimum R_{ON} of 0.57 and 0.67 mΩ cm^2, respectively, while for SBD, R_{ON} was 0.51 mΩ cm^2. In addition, from Fig. 2(a) and its inset, one can note that the JBS diodes exhibit a very high $I_F > 5.5$ kA/cm^2 at 5 V (the total current at 5 V was 0.5 A) and low V_{ON} of 0.74 V. However, the ideality factor (η) of our diodes was relatively high, around 2 [see the inset of Fig. 2(a)] probably due to the defects induced by the UHPA process.

The R_{ON} value of JBS B was higher than that of JBS A in the range V_F up to 2.5 V [see Fig. 2(a)], probably due to the shorter L_n and, thus, the higher vertical channel resistance (R_{Ch}). In the range $V_F \approx 2.5$–3 V, R_{ON} of the JBS B decreases to the level of the SBD diode [Fig. 2(a)]. This suggests that some of the metal p-GaN contacts in the JBS B could be rather Ohmic-like but not Schottky ones because the range of V_F from 2.5 to 3 V corresponds to the turn-on voltage of GaN pn diodes. However, as we mentioned previously, the Ohmic contacts were poor. Thus, the reason for this issue is rather not clear at this moment. Another interesting problem is decreasing of the slope of I_F–V_F curves above $V_F > 3$ V for all diodes (an increase in R_{ON}), as can be seen in Fig. 2(a). Previously, such a phenomenon was observed for SiC and Ga_2O_3 SBD/JBS diodes[42,43] and attributed to the self-heating effect (Joule heat generation). More precisely, when high I_F is reached the SBD diode (in the case of the SiC SBD, it is of the order of magnitude of kA/cm^2), the Joule heat is generated, which leads to a significant increase in the lattice temperature and large degradation in the carriers mobility. As a consequence, R_{ON} increases and the slope of the I_F–V_F curve decreases, as shown in Fig. 2(a). However, in the case of GaN based SBD diodes, the decrease in slope of the I_F–V_F curve is not often observed for V_F up to 5 V, and thus, the question arises why this phenomenon occurred in the fabricated diodes. The simple answer is that this is a direct consequence of low R_{ON} of our diodes. Namely, due to low R_{ON}, the amount of Joule heat ($Q = V_F^2 t / R_{ON}$, where t is the time) generated in our diodes starts to be significant already at relatively low V_F, which causes degradation in the carrier mobility the carriers mobility and the decrease in the slope of the I_F–V_F curve.

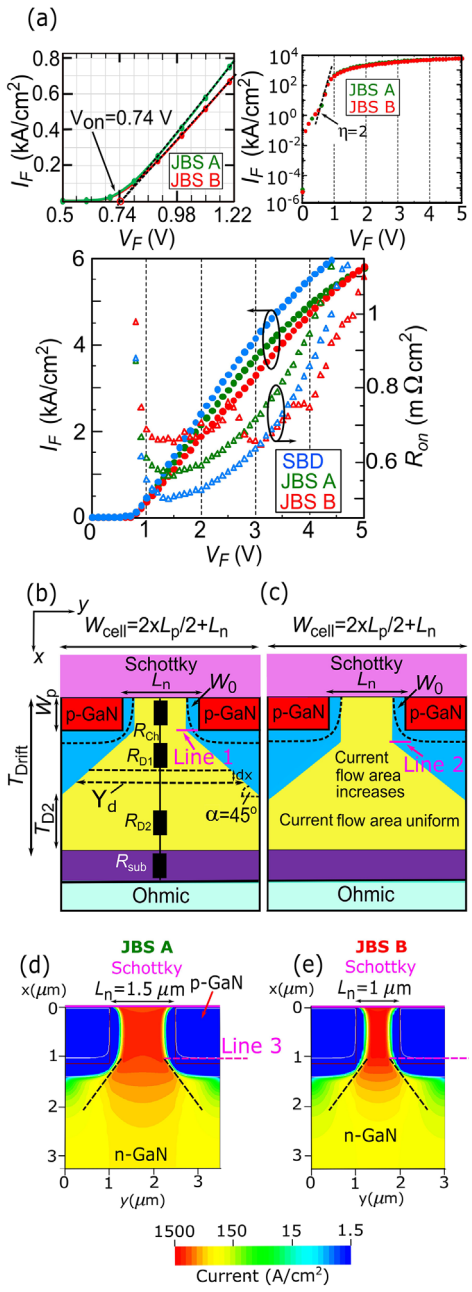

FIG. 2. (a) Linear-scale I_F–V_F curves of SBD and JBS diodes and corresponding R_{ON}. Current distributions in the JBS diode: (b) the start of current spreading from the end of the pn junction (line 1) and (c) the start of current spreading from the end of the depletion region (line 2). Two-dimensional (2D) current density distribution in (d) JBS A and (e) JBS B at $V_F = 1$ V. Inset of Fig. 2a shows the linear-scale I_F–V_F characteristics at V_F range from 0.5 to 1.22 V and semilog I_F–V_F curves of JBS diodes.

The difference between R_{ON} of JBS diodes and SBD ones can be explained using the following R_{ON} model. The R_{ON} of the JBS diode contains the series of various resistances, as shown in Fig. 2(b) and can be given by

$$R_{ON} = R_{Ch} + R_{Drift} + R_{Sub} + R_{Con}, \quad (1)$$

where R_{Drift}, R_{Sub}, and R_{Con} are the drift layer resistance, substrate resistance, and contact resistance, respectively. The R_{Con} is typically much lower than R_{Sub} and, thus, can be neglected. For the calculations of JBS R_{ON}, two scenarios of the current distribution can be adopted. In the first one, the current spreading starts from the end of the pn junction [line 1 in Fig. 2(b)] (similar like in VD-MOSFET, see Ref. 44) while in the second scenario, the current spreading starts from the end of the depletion region [see line 2 in Fig. 2(c)] (similar like in SiC JBS diodes, see Refs. 45, 46). According to the TCAD simulation, in the case of the fabricated JBS diodes, the current spreading starts from line 3 [see Figs. 2(d) and 2(e)], which is close to line 1 [see Fig. 2(b)]. This means that the current distribution from Fig. 2(b) is more adequate to our JBS diodes, and thus, R_{Ch} can be calculated similarly like the JFET resistance in VD-MOSFET [see Eq. (6.72) in Ref. 44]

$$R_{Ch} = \frac{\varrho W_{Cell} W_p}{L_n - 2 \times W_0}, \quad (2)$$

where ϱ is the resistivity of the n-GaN region, W_{Cell}=$2 \times L_p/2 + L_n$ is the cell width, W_p is the p–n junction depth, and W_0 is the depletion region width at 0 V bias [Fig. 2(b)]. The R_{Drift} in the case of the JBS structure is expected to be different than in the case of SBD due to the current spreading from the n-GaN channel, as shown in Fig. 2(c). Assuming the 45° spreading angle, R_{Drift} of the JBS diode is determined by the region where the current flow area increases [Fig. 2(c)] and the region where the current flow area is uniform [Fig. 2(c)]. The relationship for the resistance of a layer, in which the current flow is non-uniform, R_{D1} is obtained by the integration of the resistance of an elemental segment with thickness dx and width $Yd = a + 2x$ [see Fig. 2(b)] over the limits $x = 0$ and $x = (W_{Cell} - a)/2$, where $a = L_n - 2 \times W_0$

$$R_{D1} = \int dR_{D1} = \int W_{Cell} \varrho \frac{dy}{a + 2x} = \frac{\varrho W_{Cell}}{2} \ln \left[\frac{W_{Cell}}{L_n - 2 \times W_0} \right]. \quad (3)$$

Note that the above equation was multiplied by the cell area.

On the other hand, the resistance of the layer in which the current flow is uniform, R_{D2} is determined by the calculation of the thickness of this layer [T_{D2}, see Fig. 2(b)]. By the simple consideration of a 45° triangle from Fig. 2(b), we obtain that T_{D2} is equal

$$T_{D2} = T_{Drift} + \frac{L_n}{2} - W_0 - \frac{W_{Cell}}{2}, \quad (4)$$

where T_{Drift} is the drift layer thickness. Thus, R_{D2} is given by

$$R_{D2} = \varrho L_{D2} = \varrho \left[T_{Drift} + \frac{L_n}{2} - W_0 - \frac{W_{Cell}}{2} \right]. \quad (5)$$

Finally, R_{Drift} is the sum of R_{D1} and R_{D2},

$$R_{Drift} = R_{D1} + R_{D2} = \frac{\varrho W_{Cell}}{2} \ln \left[\frac{W_{Cell}}{L_n - 2 \times W_0} \right] + \varrho \left[(T_{Drift} + \frac{L_n}{2} - W_0 - \frac{W_{Cell}}{2} \right]. \quad (6)$$

All the parameters in Eqs. (1)–(6) are known expect from ϱ which can be determined from R_{ON} of SBD. Namely, R_{ON} of SBD is given by the relationship (after neglecting R_{Con})

$$R_{ON} = R_{DS} + R_{Sub}, \quad (7)$$

where $R_{DS} = \varrho T_{Drift}$ is the drift layer resistance of SBD. The R_S value for the used GaN substrate was estimated as 0.294 ± 0.023 mΩ cm^2, and thus from Eq. (7), we obtained $\varrho = 217 \pm 23$ mΩ cm (assuming $R_{ON} = 0.51$ mΩ cm^2 of SBD). The ϱ range of 194–240 mΩ cm corresponds to the average mobility $\mu = 1/(qN_D\varrho) = 1166 \pm 124$ cm^2/V s, which is reasonable for the GaN layer with $N_d = 2.5 \times 10^{16}$ cm^{-3} grown on a GaN substrate.[47] In order to improve the accuracy of the R_{Ch} estimations, we used the L_n determined based on SCM data [see discussion on Figs. 1(d) and 1(e)]. For the JBS A, average $L_n \approx 1.36$ and $W_{Cell} = 3.5\ \mu$m, while for JBS B, average $L_n \approx 0.86$ and $W_{Cell} = 3\ \mu$m. Thus, after introducing these parameters to Eqs. (1)–(6) together with $\varrho = 220$ mΩ cm, $T_{Drift} = 10\ \mu$m, and $W_0 = 0.31\ \mu$m (calculated assuming the graded p–n junction, see the supplementary material), and $W_p = 1.1\ \mu$m [see the SIMS profile, Fig. 1(b), point where [Mg] = N_d], we obtained that R_{ON} of the JBS A and B is ≈0.64 and 0.86 mΩ cm^2, respectively. These values are in good agreement with the experimental ones (0.57 and 0.67 mΩ cm^2). Based on these results, we can conclude that the increases in R_{ON} of both JBS diodes with respect to SBD are mainly due to R_{Ch}. The difference between the experimental and theoretical R_{ON} values is probably due to overestimation of the Mg lateral diffusion from the SCM analysis [Fig. 1(e)] and not accurate estimation of ϱ (194–240 mΩ cm). If we assume the lack of Mg lateral diffusion, i.e., L_n values as designed [see Fig. 1(a)] and $\varrho = 194$ mΩ cm, we obtain the R_{ON} values almost the same as experimental ones, i.e., 0.59 mΩ cm^2 2 (JBS A) and 0.69 mΩ cm^2 (JBS B). These results suggest that the EJ locations [see Fig. 1(e)] are manly affected by the AC tip bias.

Figure 3(a) shows the representative I_R–V_R characteristics of the JBS diodes, SBDs, and implanted p–n diodes. The I_R–V_R were obtained using the fluorinert. On can note the large improvement of the reverse characteristics of the JBS diodes with respect to SBD. In particular, the SBD exhibited the BV of 120 V while the JBS diodes BV of 660–675 V (84.4% of ideal BV = 800 V for $N_D = 2.5 \times 10^{16}$ cm^{-3}; more details on the ideal BV, one can find in Ref. 34), which is close to the implanted p–n diode. The maximal electric field (E_{max}) at the breakdown (estimated according to Ref. 13) was $E_{max} > 2.47$ MV/cm (for JBS A), which is consistent with E_{max} reported by Maeda *et al.*[34,48,49] for $N_d = 2.5 \times 10^{16}$ cm^{-3}. Furthermore, compared to SBDs, the JBS devices had much lower leakage currents (by the factor of 10^3–10^4 orders of magnitude) at $V_R = 120$ V. It is interesting also to note that the leakage currents in the JBS B are one order of magnitude lower than in JBS A. Moreover, the behavior of the leakage currents as a function of V_R is slightly different between the JBS diodes A and B. The leakage currents in the JBS A initially increase like in SBD while in the JBS B such an initial increase is not observed [Fig. 3(a)]. To understand this discrepancy, we simulated the two-dimensional (2D) electric field distribution in the JBS A and B, as shown in Figs. 3(b) and 3(c) under $V_R = 200$ V. It is clear that in the case of the JBS B, the electric field in the n-GaN channel near the Schottky interface is significantly lower than in the JBS A. This is because in the JBS B, the p-type regions are much closer than in the JBS A with more effectively depleted n-GaN channel and, thus, reduced electric field near the

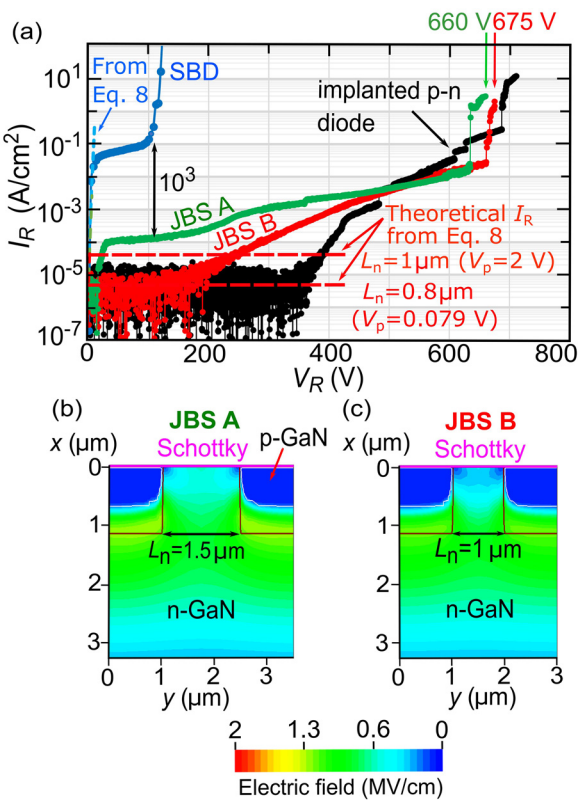

FIG. 3. (a) I_R–V_R characteristics of SBD, JBS, and p–n diodes and calculated 2D electric field distributions in JBS A (b) and (c) B at $V_R = 200$ V. Dashed lines were calculated using Eq. (8).

Schottky interface. Due to the lower electric field near the Schottky interface, TFE in the JBS B is more suppressed compared to the JBS A, which results in the lower leakage currents and weaker V_R dependencies. An additional finding in Fig. 3(a) is that the pn diode exhibits the higher leakage current than JBS diodes at bias larger than 500 V. We attributed this phenomenon to the Mg condensation at threading dislocations[47] (TSDs), which is more probable in the pn diodes than in JBS ones because of much larger implanted Mg areas. Finally, it is important to note that the I_R-V_R characteristics of our JBS diodes can be excellently explained using a well verified reverse leakage model of the JBS diode.[45,46] According to this model, I_R of the JBS diode is given by

$$I_R = \frac{L_n}{W_{Cell}} A_R T^2 \exp\left(-\frac{q\Phi}{kT}\right) \exp\left(\frac{q^{\frac{3}{2}} E_{JBS}^{\frac{1}{2}}}{(4\pi\varepsilon_s)^{\frac{1}{2}} kT}\right) \exp\left(CE_{JBS}^2\right), \quad (8)$$

where A_R is the Richardson constant equal to 24 A/(K^2 cm^2), ε_s is the dielectric constant of GaN with the relative permittivity of 10.4, C is the tunneling constant, Φ is the SBD barrier height, and E_{JBS} is the electric field in the Schottky region given by

$$E_{JBS} = \sqrt{\frac{2qN_d}{\varepsilon_s}(V_R + V_b)}, \quad (9)$$

where V_b is the Schottky contact potential.

When V_R exceeds the pinch-off voltage $V_P = \frac{Ln^2 qN_d}{8\varepsilon_s} - V_B$ [where V_B is the built-in voltage of the p–n junction (3.4 V)], E_{JSB} and, thus, I_R of JBS become approximately constant due to the channel pinch-off effect. From fitting of the experimental I_R for a simple SBD in Eq. (8) [see Fig. 3(a)](without the L_n/W_{Cell} factor), we determined $\Phi = 0.7$ V and $C = 10^{-10}$ cm^2/V^2. We used these parameters to calculate I_R of JBS diodes using Eq. (8). As can be seen from Fig. Fig. 3(a), when we assume L_n values very close to the designed ones, i.e., 0.8 μm ($V_P = 0.079$ V) for JBS diode B, the calculated I_R is in excellent agreement with experimental data. Furthermore, for JBS B, if we assume the exact designed L_n value of 1 μm ($V_P = 2$ V), I_R is also consistent with experimental one [see Fig. 3(a)]. This means that I_R of the JBS diodes can be well explained only by variations of the L_n parameter.

Figure 4 shows the I_R–V_R characteristics of JBS A after several repetitive measurements. The diode showed no destruction against the rapid increase in I_R above two orders of magnitude up to 3 A/cm^2. Unfortunately, the temperature dependencies of the I_R–V_R characteristics were difficult to obtain since BV of the JBS diodes was very sensitive to the presence of the fluorinert medium, which evaporates at elevated temperatures (without the fluorinert medium, the BV of JBS diodes was below 500 V, see Fig. 4). Figure 5 shows the dependencies of R_{ON} vs BV of GaN-based quasi and vertical SBDs and GaN p–n diodes with BV of 700 V. The figure of merit of the fabricated JBS diodes was from 0.68 to 0.76 GW/cm^2, which is one of the highest values reported so far for GaN SBDs. Furthermore, R_{ON} of our JBS diodes is the lowest among all reported so far for the vertical GaN SBDs and is comparable with R_{ON} of vertical GaN p–n diodes with the BV of 630–720 V. It should also be highlighted that R_{ON} of JBS diodes will still be a record low even if I_F of JBS diodes is normalized to the total JBS device area of 9.7×10^{-5} cm^2 (i.e., the Schottky metal area plus edge termination area). In this case, R_{ON} will be 0.64 mΩ cm^2 for JBS A and 0.75 mΩ cm^2 for JBS B.

In conclusion, we demonstrated the Mg-implanted GaN vertical JBS diodes fabricated using the UHPA method, which exhibit superior electrical characteristics and nondestructive breakdown. The JBS diodes have the record low R_{ON} in the range from 0.57 to 0.67 mΩ cm^2, high BV in the range from 660 to 675 V and low V_{ON} of 0.74 V. In addition, the JBS diodes showed a very high $I_F > 5$ kA/cm^2 and relatively low leakage currents. This work showed that GaN JBS diodes can be strong candidates for low loss power switching applications.

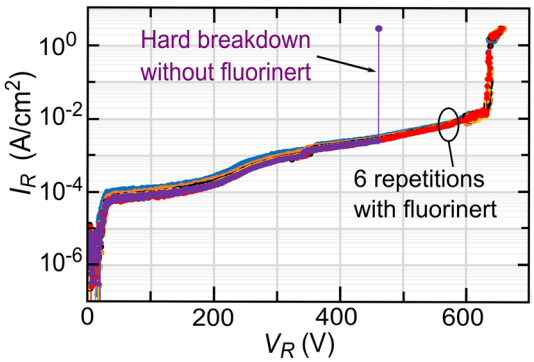

FIG. 4. I_R–V_R characteristics of the JBS diode after several-time repeated treatment using the flourinert and I_R–V_R characteristics of the same diode obtained without flourinert.

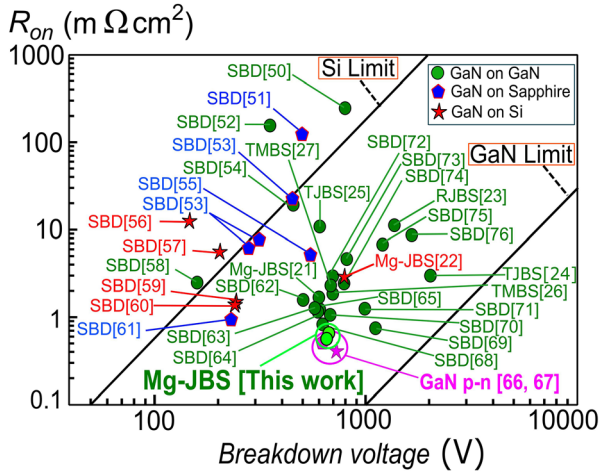

FIG. 5. R_{ON}–BV benchmark comparison among most GaN SBDs,[50–65,68–76] Mg-implanted JBS,[21,22] regrowth JBS (RJBS),[23] trench JBS (TJBS),[24,25] TMBS,[26,27] and p–n diodes (PNDs)[66,67] with the BV of 630–720 V. Our JBS diodes demonstrate the lowest R_{ON} for vertical SBDs, which are comparable with R_{ON} of GaN p–n diodes.

See the supplementary material for estimations of the electrical junction location (Fig. S1) and depletion layer width at the zero bias (Fig. S2) from TCAD simulations.

This work was supported by the Ministry of Education, Culture, Sports, Science and Technology (MEXT) "Research and development of next-generation semiconductor to realize energy-saving society" Program via Grant No. JPJ005357 and the MEXT-Program for the Creation of Innovative Core Technology for Power Electronics via Grant No. JPJ009777. The authors thank the Center for Integrated Research of Future Electronics, Transformative Electronics Facilities (C-TEFs) at Nagoya University for helping to fabricate the devices used in this work. The authors thank Dr. Masakazu Kanechika of Nagoya University for his kind support during the experiment.

AUTHOR DECLARATIONS

Conflict of Interest

The authors have no conflicts to disclose.

Author Contributions

Maciej Franiczek Matys: Conceptualization (lead); Data curation (equal); Formal analysis (lead); Investigation (equal); Methodology (equal); Software (lead); Validation (equal); Visualization (equal); Writing – original draft (lead); Writing – review & editing (lead). **Kazuki Kitagawa:** Conceptualization (supporting); Data curation (supporting); Formal analysis (supporting); Investigation (supporting); Methodology (supporting); Resources (supporting); Software (equal); Validation (supporting); Visualization (supporting); Writing – original draft (supporting); Writing – review & editing (supporting). **Tetsuo Narita:** Conceptualization (equal); Data curation (equal); Formal analysis (equal); Investigation (equal); Methodology (equal); Resources (equal); Validation (equal); Visualization (equal); Writing – original draft (equal); Writing – review & editing (equal). **Tsutomu Uesugi:** Conceptualization (equal); Data curation (equal); Formal analysis (equal); Investigation (equal); Methodology (equal); Resources (equal); Validation (equal); Visualization (equal); Writing – original draft (equal); Writing – review & editing (equal). **Jun Suda:** Conceptualization (equal); Data curation (equal); Formal analysis (equal); Funding acquisition (equal); Investigation (equal); Methodology (equal); Project administration (lead); Resources (equal); Supervision (lead); Validation (equal); Visualization (equal); Writing – original draft (equal); Writing – review & editing (equal). **Tetsu Kachi:** Conceptualization (lead); Data curation (equal); Formal analysis (equal); Funding acquisition (equal); Investigation (equal); Methodology (equal); Project administration (lead); Resources (equal); Supervision (lead); Validation (equal); Visualization (equal); Writing – original draft (equal); Writing – review & editing (equal).

DATA AVAILABILITY

The data that support the findings of this study are available from the corresponding author upon reasonable request.

REFERENCES

[1]H. Amano, Y. Baines, E. Beam, M. Borga, T. Bouchet, P. R. Chalker, M. Charles, K. J. Chen, N. Chowdhury, R. Chu, C. De Santi, M. M. De Souza, S. Decoutere, L. D. Cioccio, B. Eckardt, T. Egawa, P. Fay, J. J. Freedsman, L. Guido, O. Häberlen, G. Haynes, T. Heckel, D. Hemakumara, P. Houston, J. Hu, M. Hua, Q. Huang, A. Huang, S. Jiang, H. Kawai, D. Kinzer, M. Kuball, A. Kumar, K. B. Lee, X. Li, D. Marcon, M. März, R. McCarthy, G. Meneghesso, M. Meneghini, E. Morvan, A. Nakajima, E. M. S. Narayanan, S. Oliver, T. Palacios, D. Piedra, M. Plissonnier, R. Reddy, M. Sun, I. Thayne, A. Torres, N. Trivellin, V. Unni, M. J. Uren, M. Van Hove, D. J. Wallis, J. Wang, J. Xie, S. Yagi, S. Yang, C. Youtsey, R. Yu, E. Zanoni, S. Zeltner, and Y. Zhang, J. Phys. D **51**, 163001 (2018).
[2]T. Kachi, Jpn. J. Appl. Phys., Part 1 **53**, 100210 (2014).
[3]T. Kachi, "GaN devices for automotive application and their challenges in adoption," in IEEE International Electron Devices Meeting (IEDM), 2018.
[4]T. Narita, H. Yoshida, K. Tomita, K. Kataoka, H. Sakurai, M. Horita, M. Bockowski, N. Ikarashi, J. Suda, T. Kachi, and Y. Tokuda, J. Appl. Phys. **128**, 090901 (2020).
[5]T. Oka, Jpn. J. Appl. Phys., Part 1 **58**, SB0805 (2019).
[6]M. Meneghini, C. De Santi, I. Abid, M. Buffolo, M. Cioni, R. A. Khadar, L. Nela, N. Zagni, A. Chini, F. Medjdoub, G. Meneghesso, G. Verzellesi, E. Zanoni, and E. Matioli, J. Appl. Phys. **130**, 181101 (2021).
[7]K. J. Chen, O. Häberlen, A. Lidow, C. lin Tsai, T. Ueda, Y. Uemoto, and Y. Wu, IEEE Trans. Electron Devices **64**, 779 (2017).
[8]Y. Zhang, A. Dadgar, and T. Palacios, J. Phys. D **51**, 273001 (2018).
[9]D. Khachariya, D. Szymanski, P. Reddy, E. Kohn, Z. Sitar, R. Collazo, and S. Pavlidis, ECS Trans. **98**, 69 (2020).
[10]T. Ueda, M. Ishida, T. Tanaka, and D. Ueda, Jpn. J. Appl. Phys., Part 1 **53**, 100214 (2014).
[11]T. Ishida, K. Pil Nam, M. Matys, T. Uesugi, J. Suda, and T. Kachi, Appl. Phys. Express **13**, 124003 (2020).
[12]Y. Sun, X. Kang, Y. Zheng, J. Lu, X. Tian, K. Wei, H. Wu, W. Wang, X. Liu, and G. Zhang, Electronics **8**(5), 575 (2019).
[13]I. C. Kizilyalli, A. P. Edwards, H. Nie, D. Disney, and D. Bour, IEEE Trans. Electron Devices **60**, 3067 (2013).
[14]I. C. Kizilyalli, A. P. Edwards, H. Nie, D. Bour, T. Prunty, and D. Disney, IEEE Electron Device Lett. **35**, 247 (2014).
[15]I. C. Kizilyalli, T. Prunty, and O. Aktas, IEEE Electron Device Lett. **36**, 1073 (2015).

[16]O. Aktas and I. C. Kizilyalli, IEEE Electron Device Lett. **36**, 890 (2015).
[17]H. Ohta, N. Kaneda, F. Horihiri, Y. Nirita, T. Yoshida, T. Mishima, and T. Nakamura, IEEE Electron Device Lett. **36**, 1180 (2015).
[18]H. Ohta, K. Hayashi, F. Horikiri, M. Yoshino, T. Nakamura, and T. Mishima, Jpn. J. Appl. Phys., Part 1 **57**, 04FG09 (2018).
[19]Z. Bian, K. Zeng, and S. Chowdhury, IEEE Electron Device Lett. **43**, 596 (2022).
[20]D. Koehler, T. J. Anderson, M. J. Tadjer, A. Nath, B. N. Feigelson, D. I. Shahin, K. D. Hobart, and F. J. Kuba, ECS J. Solid State Sci. Technol. **6**, Q10 (2017).
[21]Y. Zhang, Z. Liu, M. J. Tadjer, M. Sun, D. Piedra, C. Hatem, T. J. Anderson, L. E. Luna, A. Nath, A. D. Koehler, H. Okumura, J. Hu, X. Zhang, X. Gao, B. N. Feigelson, K. D. Hobart, and T. Palacios, IEEE Electron Device Lett. **38**, 1097 (2017).
[22]F. Zhou, W. Xu, F. Ren, D. Zhou, D. Zhou, D. Chen, R. Zhang, Y. Zheng, T. Zhu, and H. Lu, IEEE Trans. Power Electron. **36**, 12163 (2021).
[23]A. T. Binder, G. W. Pickrell, A. A. Allerman, J. R. Dickerson, L. Yates, J. Steinfeldt, C. Glaser, M. H. Crawford, A. Armstrong, P. Sharps, and R. J. Kaplar, "Etched and regrown vertical GaN junction barrier Schottky diodes," in *IEEE 8th Workshop on Wide Bandgap Power Devices and Applications (WiPDA)* (IEEE, 2021), pp. 288–292.
[24]T. Hayashida, T. Nanjo, A. Furukawa, and M. Yamamuka, Appl. Phys. Express **10**, 061003 (2017).
[25]W. Li, K. Nomoto, M. Pilla, M. Pan, X. Gao, D. Jena, and H. G. Xing, IEEE Trans. Electron. Devices **64**, 1635 (2017).
[26]K. Hasegawa, G. Nishio, K. Yasunishi, N. Tanaka, N. Murakami, and T. Oka, Appl. Phys. Express **10**, 121002 (2017).
[27]Y. Zhang, M. Sun, Z. Liu, D. Piedra, M. Pan, X. Gao, Y. Lin, A. Zubair, L. Yu, and T. Palacios, "Novel GaN trench MIS barrier Schottky rectifiers with implanted field rings," in IEEE International Electron Devices Meeting (IEDM), 2016.
[28]M. Matys, T. Ishida, K. Nam, H. Sakurai, T. Narita, T. Uesugi, M. Bockowski, J. Suda, and T. Kachi, Appl. Phys. Lett. **118**, 093502 (2021).
[29]M. Matys, T. Ishida, K. Nam, H. Sakurai, K. Kataoka, T. Narita, T. Uesugi, M. Bockowski, M. Nishimura, J. Suda, and T. Kachi, Appl. Phys. Express **14**, 074002 (2021).
[30]H. Sakurai, M. Omori, S. Yamada, Y. Furukawa, H. Suzuki, T. Narita, K. Kataoka, M. Horita, M. Bockowski, J. Suda, and T. Kachi, Appl. Phys. Lett. **115**, 142104 (2019).
[31]H. Sakurai, T. Narita, M. Omori, S. Yamada, A. Koura, M. Iwinska, K. Kataoka, M. Horita, N. Ikarashi, M. Bockowski, J. Suda, and T. Kachi, Appl. Phys. Express **13**, 086501 (2020).
[32]K. Sierakowski, R. Jakiela, B. Lucznik, P. Kwiatkowski, M. Iwinska, M. Turek, H. Sakurai, T. Kachi, and M. Bockowski, Electronics **9**, 1380 (2020).
[33]M. H. Breckenridge, J. Tweedie, P. Reddy, Y. Guan, P. Bagheri, D. Szymanski, S. Mita, K. Sierakowski, M. Bockowski, R. Collazo, and Z. Sitar, Appl. Phys. Lett. **118**, 022101 (2021).
[34]T. Maeda, T. Narita, S. Yamada, T. Kachi, T. Kimoto, M. Horita, and J. Suda, J. Appl. Phys. **129**, 185702 (2021).
[35]S. Mandal, A. Agarwal, E. Ahmadi, K. M. Bhat, D. Ji, M. A. Laurent, S. Keller, and S. Chowdhury, IEEE Electron Device Lett. **38**(7), 933–936 (2017).
[36]T. Nishimura and T. Kachi, Appl. Phys. Express **14**, 116502 (2021).
[37]A. Uedono, R. Tanaka, S. Takashima, K. Ueno, M. Edo, K. Shima, K. Kojima, S. F. Chichibu, and S. Ishibashi, Sci. Rep. **11**, 20660 (2021).
[38]M. Akazawa, R. Kamoshida, S. Murai, T. Kachi, and A. Uedono, Jpn. J. Appl. Phys., Part 1 **60**, 016502 (2021).
[39]M. L. O'Malley, G. L. Timp, S. V. Moccio, J. P. Garno, and R. N. Kleiman, Appl. Phys. Lett. **74**, 272 (1999).
[40]P. Fiorenza, M. S. Alessandrino, G. Carbone, A. Russo, F. Roccaforte, and G. Giannazzo, Nanomaterials **11**, 1626 (2021).
[41]M. L. O'Malley, G. L. Timp, W. Timp, S. V. Moccio, J. P. Garno, and R. N. Kleiman, Appl. Phys. Lett. **74**, 3672 (1999).
[42]R. Sharma, E. Patrick, M. E. Law, J. Yang, F. Ren, and S. J. Pearton, ECS J. Solid State Sci. Technol. **8**, Q3195 (2019).
[43]R. Pérez, N. Mestres, M. VellVehí, P. Godignon, and J. Millán, Semicond. Sci. Technol. **21**, 670 (2006).
[44]B. Baliga, *Fundamentals of Power Semiconductor Devices* (Springer International Publishing, 2019).
[45]B. J. Baliga, *Advanced Power Rectifier Concepts* (Springer US, 2009).
[46]B. J. Baliga, *Gallium Nitride and Silicon Carbide Power Devices* (World Scientific Publishing Company, 2016).
[47]T. Narita and Y. Tokuda, "Deep levels in GaN," in *Characterization of Defects and Deep Levels for GaN Power Devices*, edited by T. Narita and T. Kachi (AIP Publishing, Melville, New York, 2020), Chap. 3, pp. 3–12.
[48]T. Maeda, T. Narita, H. Ueda, M. Kanechika, T. Uesugi, T. Kachi, T. Kimoto, M. Horita, and J. Suda, IEEE Electron Device Lett. **40**, 941 (2019).
[49]T. Maeda, T. Narita, S. Yamada, T. Kachi, T. Kimoto, and M. Horita, in *IEEE International Electron Devices Meeting, Technical Digest* (IEEE, 2019), pp. 4.2.1–4.2.4.
[50]H. Gu, C. Hu, J. Wang, Y. Lu, J.-P. Ao, F. Tian, Y. Zhang, M. Wang, X. Liu, and K. Xu, J. Alloys Compd. **780**, 476–481 (2019).
[51]A. P. Zhang, G. Dang, F. Ren, J. Han, H. Cho, S. J. Pearton, J.-I. Chyi, T.-E. Nee, C. M. Lee, C. C. Chuo, and S. N. G. Chu, Solid-State Electron. **44**, 1157 (2000).
[52]S.-C. Lee, J.-C. Her, S.-S. Kim, M.-W. Ha, K.-S. Seo, Y.-I. Choi, and M.-K. Han, "A new vertical GaN Schottky barrier diode with floating metal ring for high breakdown voltage," in *Proceedings of the 16th International Symposium on Power Semiconductor Devices and ICs* (IEEE, 2004), pp. 319–322.
[53]T. G. Zhu, D. J. H. Lambert, B. S. Shelton, M. M. Wong, V. Chowdhury, and R. D. Dupuis, Appl. Phys. Lett. **77**, 2918 (2000).
[54]J. W. Johnson, J. R. Laroche, F. Ren, B. P. Gila, M. E. Overberg, C. R. Abernathy, J. I. Chyi, C. C. Chuo, T. E. Nee, C. M. Lee, K. P. Lee, S. S. Park, Y. J. Park, and S. J. Pearton, Solid-State Electron. **45**, 405–410 (2001).
[55]G. T. Dang, A. P. Zhang, M. M. Mshewa, and F. Ren, J. Vac. Sci. Technol. A **18**, 1135 (2000).
[56]K. Zhang, S. Mase, K. Nakamura, T. Hamada, and T. Egawa, Electron. Lett. **53**, 1610–1611 (2017).
[57]Y. Zhang, M. Sun, D. Piedra, M. Azize, X. Zhang, T. Fujishima, and T. Palacios, IEEE Electron Device Lett. **35**, 618 (2014).
[58]K. Ip, K. H. Baik, B. Luo, F. Ren, S. J. Pearton, S. S. Park, Y. J. Park, and A. P. Zhang, Solid-State Electron. **46**, 2169 (2002).
[59]C. Liu, R. Abdul Khadar, and E. Matioli, IEEE Electron Device Lett. **39**, 1034 (2018).
[60]X. Guo, Y. Zhong, J. He, Y. Zhou, S. Su, X. Chen, J. Liu, H. Gao, X. Sun, Q. Zhou, Q. Sun, and H. Yang, IEEE Electron Device Lett. **42**, 473 (2021).
[61]W. Witte, D. Fahle, H. Koch, M. Heuken, H. Kalisch, and A. Vescan, Semicond. Sci. Technol. **27**, 085015 (2012).
[62]H. Fu, X. Huang, H. Chen, Z. Lu, I. Baranowski, and Y. Zhao, Appl. Phys. Lett. **111**, 152102 (2017).
[63]S. Hashimoto, Y. Yoshizumi, T. Tanabe, and M. Kiyama, J. Cryst. Growth **298**, 871 (2007).
[64]Y. Wang, S. Alur, Y. Sharma, F. Tong, R. Thapa, P. Gartland, T. Issacs-Smith, C. Ahyi, J. Williams, M. Park, M. Johnson, T. Paskova, E. A. Preble, and K. R. Evans, Semicond. Sci. Technol. **26**, 022002 (2011).
[65]D. Disney, H. Nie, A. Edwards, D. Bour, H. Shah, and I. C. Kizilyalli, "Vertical power diodes in bulk GaN," in *Proceedings of the International Symposium on Power Semiconductor Devices and ICs* (IEEE, 2013), pp. 59–62.
[66]B. S. Zheng, P. Y. Chen, C. J. Yu, Y. F. Chang, C. L. Ho, M. C. Wu, and K. C. Hsieh, IEEE Electron Device Lett. **36**, 932 (2015).
[67]Y. Zhang, M. Yuan, N. Chowdhury, K. Cheng, and T. Palacios, IEEE Electron Device Lett. **39**, 715 (2018).
[68]M. Ueno, S. Yoshimoto, K. Ishihara, M. Okada, K. Sumiyoshi, H. Hirano, F. Mitsuhashi, Y. Yoshizumi, T. Ishizuka, and M. Kiyama, "Fast recovery performance of vertical GaN Schottky barrier diodes on low-dislocation-density GaN substrates," in *Proceedings of the IEEE 26th International Symposium on Power Semiconductor Devices and IC's (ISPSD), Waikoloa, HI* (2014).
[69]Y. Saitoh, K. Sumiyoshi, M. Okada, T. Horii, T. Miyazaki, H. Shiomi, M. Ueno, K. Katayama, M. Kiyama, and T. Nakamura, Appl. Phys. Express **3**, 081001 (2010).
[70]T. Horii, T. Miyazaki, Y. Saito, S. Hashimoto, T. Tanabe, and M. Kiyama, "High-breakdown-voltage gan vertical Schottky barrier diodes with field plate structure," Mater. Sci. Forum **615–617**, 963–966 (2009).
[71]S. Han, S. Yang, and K. Sheng, IEEE Electron Device Lett. **39**(4), 572–575 (2018).
[72]Y. Zhou, D. Wang, C. Ahyi, C.-C. Tin, J. Williams, M. Park, N. M. Williams, and A. Hanser, Solid-State Electron. **50**, 1744 (2006).
[73]Y. Cao, R. Chu, R. Li, M. Chen, R. Chang, and B. Hughes, Appl. Phys. Lett. **108**, 062103 (2016).
[74]N. Tanaka, K. Hasegawa, K. Yasunishi, N. Murakami, and T. Oka, Appl. Phys. Express **8**, 071001 (2015).
[75]X. Liu, Q. Liu, C. Li, J. Wang, W. Yu, K. Xu, and J.-P. Ao, Jpn. J. Appl. Phys., Part 1 **56**, 026501 (2017).
[76]A. M. Ozbek and B. J. Baliga, IEEE Electron Device Lett. **32**, 300 (2011).